

Bayesian Hyperbolic Multidimensional Scaling

Bolun Liu*

Department of Biostatistics
Bloomberg School of Public Health
Johns Hopkins University

Shane Lubold
Department of Statistics
University of Washington

Adrian E. Raftery
Department of Statistics
Department of Sociology
University of Washington

Tyler H. McCormick
Department of Statistics
Department of Sociology
University of Washington

Abstract

Multidimensional scaling (MDS) is a widely used approach to representing high-dimensional, dependent data. MDS works by assigning each observation a location on a low-dimensional geometric manifold, with distance on the manifold representing similarity. We propose a Bayesian approach to multidimensional scaling when the low-dimensional manifold is hyperbolic. Using hyperbolic space facilitates representing tree-like structure common in many settings (e.g. text or genetic data with hierarchical structure). A Bayesian approach provides regularization that minimizes the impact of uncertainty or measurement error in the observed data. We also propose a case-control likelihood approximation that allows for efficient sampling from the posterior in larger data settings, reducing computational complexity from approximately $O(n^2)$ to $O(n)$. We evaluate the proposed method against state-of-the-art alternatives using simulations, canonical reference datasets, and human gene expression data. Code to reproduce the result in the paper are available at <https://github.com/peterliu599/BHMDS>.

Keywords: Bayesian methods, Hyperbolic geometry, Multidimensional scaling

1 Introduction

Multidimensional scaling (MDS) methods represent high-dimensional data in a low-dimensional space, using dissimilarities between the observations as a means of identifying positions (Kruskal,

*The authors gratefully acknowledge support from NIH grants R01 HD070936 (Raftery) and DP2 MH122405 (McCormick). Correspondence: tylermc@uw.edu.

1964). Observations with small dissimilarities will be placed close together, while those with larger dissimilarities will be placed further apart. A long literature on MDS methodology illustrates the utility of MDS as a means of summarizing complex, dependent data and for downstream applications, such as detecting clusters from the dissimilarities (Borg and Groenen, 1997; Davison, 1983; Cox and Cox, 2001).

In many settings, the observed dissimilarities we wish to apply MDS methods to are likely to contain measurement error. These errors could arise from misreporting in the context of the social sciences (e.g. a retrospective behavioral inventory) or from miscalibration of machinery or operator error in industrial settings. Using a probabilistic model is one way to account for this additional uncertainty. Takane and Carroll (1981); Groenen (1993); MacKay (1989) and others have proposed maximum likelihood MDS methods for handling measurement error. The use of these methods relies on asymptotic theory, which might not apply for sample sizes used in applications, and the problem requires solving a non-linear optimization problem where the number of parameters grows quickly as the sample size grows (Cox and Cox, 2001). One potential framework to address these potential issues with MDS is a Bayesian framework. Oh and Raftery (2001) provided a Bayesian procedure to estimate the configuration of objects given (potentially noisy) dissimilarities between objects. Extensions of Bayesian MDS to the case of large datasets were discussed in Holbrook *et al.* (2021).

Along with the statistical framework, another critical, but often ignored, choice in implementing MDS is the choice of geometry for the low-dimensional manifold. Multidimensional scaling methods often assume the observed dissimilarities are computed using Euclidean distances among objects in a Euclidean space. Oh and Raftery (2001), for example, assume a Euclidean distance model with a Gaussian measurement error and propose a Markov-Chain Monte Carlo algorithm to compute a Bayesian solution for the object configuration. Yet there is a growing literature which shows that representing objects in other embedding spaces might lead to better representations and therefore be more useful in downstream tasks (De Sa *et al.*, 2018; Chami *et al.*, 2020; Smith *et al.*, 2019; Lubold *et al.*, 2020; Keller-Ressel and Nargang, 2020). In particular, hyperbolic spaces, defined in Section 3, have been shown to produce embeddings with lower distortion, especially for data that is hierarchical or tree-like.

In this work, we combine the hyperbolic MDS methods with a Bayesian procedure. Specifically,

we apply the Bayesian MDS procedure from [Oh and Raftery \(2001\)](#) to a Hyperbolic space. We assume a Hyperbolic distance model with a Gaussian measurement error model. We then derive a Markov-chain Monte Carlo (MCMC) method we use to obtain a Bayesian solution for the object configuration in hyperbolic space.

The organization of the paper is as follows. In [Section 3](#), we formally define the Hyperbolic space model used in this work and posit a model for observed dissimilarities computed from points in a Hyperbolic space. We then discuss a prior distribution over this space and derive an MCMC algorithm to draw samples from the posterior in [Section 4](#). [Sections 5 and 6](#) contains simulations and applications of our method to real datasets in genomics. We conclude in [Section 7](#).

2 Hyperbolic Geometry

We now discuss the mathematical details of the hyperbolic geometry. The hyperbolic geometry is a non-Euclidean geometry that has a constant negative curvature, and is commonly visualized as the upper sheet of the unit two-sheet hyperboloid. There exist multiple equivalent hyperbolic models, such as the Klein model, the Poincaré disk model, and the Lorentz (Hyperboloid/Minkowski) model. We use the Lorentz model to parameterize the hyperbolic geometry, which parallels the representation used in existing hyperbolic MDS algorithms ([Keller-Ressel and Nargang, 2020](#); [De Sa et al., 2018](#)). Additionally, this representation facilitates convenient priors for our Bayesian model in [Section 3](#).

To define the Lorentz model, we begin with the definition of the Lorentzian product. For any $\mathbf{x} = (x_0, \dots, x_p)$ and $\mathbf{y} = (y_0, \dots, y_p) \in \mathbb{R}^{p+1}$, the Lorentzian product $\langle \mathbf{x}, \mathbf{y} \rangle_{\mathcal{L}}$ is defined as

$$\langle \mathbf{x}, \mathbf{y} \rangle_{\mathcal{L}} \equiv -x_0 y_0 + \sum_{i=1}^p x_i y_i .$$

The p -dimensional Lorentz model with curvature $-\kappa$, which we denote by $\mathbb{H}^p(\kappa)$, can be represented as a collection of coordinates $\mathbf{x} \in \mathbb{R}^{p+1}$ with $x_0 > 0$ such that its Lorentzian product with itself is -1 and equipped with the hyperbolic distance proportional to the square root of κ . That is,

$$\mathbb{H}^p(\kappa) \equiv \{ \mathbf{x} \in \mathbb{R}^{p+1} : x_0 > 0, \langle \mathbf{x}, \mathbf{x} \rangle_{\mathcal{L}} = -1 \}, \quad \kappa > 0 ,$$

equipped with the hyperbolic distance

$$d_{\mathbb{H}^p(\kappa)}(\mathbf{x}, \mathbf{y}) \equiv \frac{1}{\sqrt{\kappa}} \operatorname{arccosh}(-\langle \mathbf{x}, \mathbf{y} \rangle_{\mathcal{L}}), \quad (1)$$

which is the geodesic distance between \mathbf{x} and \mathbf{y} on $\mathbb{H}^p(\kappa)$. Specifically, the curvature $-\kappa$ controls the hyperbolicity of the geometry, so that the space becomes more hyperbolic as $-\kappa$ becomes more negative and becomes flatter as κ shrinks to zero (Euclidean geometry has curvature exactly 0).

3 Bayesian Modeling Framework

We now describe our statistical framework for Bayesian Hyperbolic Multidimensional Scaling (BHMDs), which represents the objects of interest by coordinates in a hyperbolic geometry, so that the hyperbolic distances between objects resemble their true dissimilarity measures. We suppose the objects dwell on $\mathbb{H}^p(\kappa)$ with coordinates $\mathbf{x}_1, \mathbf{x}_2, \dots, \mathbf{x}_n$, and denote by δ_{ij} the dissimilarity measure between object i and object j as well as the hyperbolic distance between \mathbf{x}_i and \mathbf{x}_j :

$$\delta_{ij} \equiv d_{\mathbb{H}^p(\kappa)}(\mathbf{x}_i, \mathbf{x}_j) = \frac{1}{\sqrt{\kappa}} \operatorname{arccos}(-\langle \mathbf{x}_i, \mathbf{x}_j \rangle_{\mathcal{L}}), \quad i, j = 1, \dots, n. \quad (2)$$

In many settings, the observed dissimilarities contain measurement errors. As in [Oh and Raftery \(2001\)](#), we represent the observed dissimilarity d_{ij} as the true dissimilarity plus a Gaussian error, with the constraint that the observed dissimilarity is always positive. We therefore assume that d_{ij} follows a truncated normal distribution:

$$d_{ij} \sim N(\delta_{ij}, \sigma^2) I(d_{ij} > 0), \quad i < j, \quad i, j = 1, \dots, n, \quad (3)$$

where δ_{ij} is as defined in (2), \mathbf{x}_i are unobserved, and σ^2 is the variance of the measurement error.

Given the statistical model, we now specify priors for $\mathbf{X} = \{\mathbf{x}_1, \dots, \mathbf{x}_n\}$ and σ^2 . Using (3), the likelihood of the unknown parameters \mathbf{X} and σ^2 is

$$l(\mathbf{X}, \sigma^2) \propto (\sigma^2)^{-m/2} \exp \left[-\frac{1}{2\sigma^2} SSR - \sum_{i < j} \log \Phi \left(\frac{\delta_{ij}}{\sigma} \right) \right],$$

where $m = n(n-1)/2$ is the number of dissimilarities, $SSR = \sum_{i < j} (\delta_{ij} - d_{ij})^2$ is the sum of squared residuals, and Φ is the cumulative distribution function of the standard normal random variable. The square-root of the SSR term in the likelihood is often referred to as *stress* in the MDS

literature, meaning that our approach falls under the umbrella of stress-minimizing approaches to MDS.

Moving now to our prior distribution choices, we use the wrapped normal distribution on $\mathbb{H}^p(\kappa)$ and centered around the hyperbolic origin (Nagano *et al.*, 2019) as the prior over the hyperbolic coordinates, \mathbf{X} . This distribution is a Gaussian-like distribution on hyperbolic geometry that is projected from \mathbb{R}^p to \mathbb{H}^p . We leverage this property to define auxiliary variables, \mathbf{v}_i , which represent coordinates in \mathbb{R}^p and define multivariate Gaussian priors over the auxiliary variables. Specifically, for a prior over the auxiliary variables \mathbf{v}_i we use a p -dimensional normal distribution with mean $\mathbf{0}_p$ and a diagonal covariance matrix Λ ($\mathbf{v}_i \sim N(0, \Lambda)$, independently for $i = 1, \dots, n$). At each step in the sampler, we transform from the Euclidean space of auxiliary variables to the Hyperbolic coordinates. We discuss the details of this transformation in the next section.

We next define the prior for the observation error variance, σ^2 . We use a conjugate prior $\sigma^2 \sim IG(a, b)$, the Inverse Gamma distribution with mode $b/(a + 1)$. For the hyperprior on the diagonal entries of the auxiliary variable variance matrix $\Lambda = \text{Diag}(\lambda_1, \dots, \lambda_p)$, we also assume a conjugate Inverse Gamma prior, $\lambda_j \sim IG(\alpha, \beta_j)$, independently for $j = 1, \dots, p$. We will further suppose prior independence among \mathbf{V} , Λ , and σ^2 , i.e., $\pi(\mathbf{V}, \sigma^2, \Lambda) = \pi(\mathbf{V})\pi(\sigma^2)\pi(\Lambda)$, where $\pi(\mathbf{V})$, $\pi(\sigma^2)$, and $\pi(\Lambda)$.

Often there is little prior information about \mathbf{V} , Λ , and σ^2 . Oh and Raftery (2001) proposed to use preliminary results from a frequentist MDS method for parameter selection in the priors, and we use a similar methodology in this study. Specifically, we use the embedding result $\mathbf{X}^{(0)} = \{\mathbf{x}_1^{(0)}, \dots, \mathbf{x}_n^{(0)}\}$ from `hydraPlus`, the stress-minimizing hyperbolic MDS algorithm proposed in Keller-Ressel and Nargang (2020), to choose the parameters of the prior distributions. For the hyperparameters of σ^2 , one can set a small a , e.g. $a = 5$, for a vague prior of σ^2 , and choose $b = (a - 1)SSR^{(0)}/m$, where $m = n(n - 1)/2$ and

$$SSR^{(0)} \equiv \sum_{i < j} \left(d_{\mathbb{H}^p(\kappa)}(\mathbf{x}_i^{(0)}, \mathbf{x}_j^{(0)}) - d_{ij} \right)^2 = \sum_{i < j} \left(\delta_{ij}^{(0)} - d_{ij} \right)^2 \quad (4)$$

is the sum of squared residuals of $\mathbf{X}^{(0)}$, so that the prior mean matches $SSR^{(0)}/m$. Similarly, for the hyperprior of λ_j , one may choose a small α , e.g. $\alpha = 0.5$, and choose β_j such that the prior mean of λ_j matches the j th diagonal element of the sample covariance matrix $S_v = \sum_{i=1}^n \mathbf{v}_i^{(0)\top} \mathbf{v}_i^{(0)}/n$, where $\mathbf{v}_i^{(0)} = T^{-1}(\mathbf{x}_i^{(0)})$ and T^{-1} the inverse transformation we describe in Section 4.1.

After specifying the prior distributions for \mathbf{V} , σ^2 , and Λ , the posterior density function of the unknown parameters \mathbf{V} , σ^2 , and Λ becomes

$$\begin{aligned} \pi(\mathbf{V}, \sigma^2, \Lambda \mid D) &\propto (\sigma^2)^{-(m/2+a+1)} \prod_{j=1}^p \lambda_j^{-n/2} \\ &\times \exp \left[-\frac{1}{2\sigma^2} SSR - \sum_{i < j} \log \Phi \left(\frac{\delta_{ij}}{\sigma} \right) - \frac{1}{2} \sum_{i=1}^n \mathbf{v}_i^\top \Lambda^{-1} \mathbf{v}_i - \frac{b}{\sigma^2} - \sum_{j=1}^p \frac{\beta_j}{\lambda_j} \right], \end{aligned} \quad (5)$$

where $D = \{d_{ij}\}_{i,j=1,\dots,n}$ is the matrix of observed dissimilarities. Due to the complex form of the posterior density function, we use a Markov-chain Monte Carlo sampler to draw from the posterior distribution.

4 Posterior Computation

After specifying the Bayesian model and prior choices, we use a Markov-chain Monte Carlo algorithm to sample from the posterior distribution. We first discuss the implementation details of the MCMC algorithm in Section 4.1. Then, in Section 4.2, we present a likelihood approximation based on work by [Raftery *et al.* \(2012\)](#) for social networks to accelerate the MCMC with large scale dissimilarity data. Specifically, we leverage the realization that the posterior likelihood can be well approximated using random samples of the objects drawn from a case-control scheme, which reduces the MCMC time complexity from $O(n^2)$ to $O(n)$.

4.1 Markov-chain Monte Carlo

Our MCMC sampler requires the hyperbolic dimension p and curvature κ as inputs. For the hyperbolic curvature κ , we can estimate $\hat{\kappa}$ using a stress minimizing algorithm which we will describe in detail in Appendix B. For the dimension, p , we could use a similar stress minimization approach across potential values of p , keeping in mind that the goal is dimension reduction so our prior is that p is much smaller than n . We could also use a Bayesian model selection approach similar to the one described by [Oh and Raftery \(2001\)](#). Given p and κ , we initialize the starting values for the MCMC sampler using the output from the `hydraPlus` algorithm. We take $\mathbf{X}^{(0)}$, $\mathbf{V}^{(0)}$, and $\{\delta_{ij}^{(0)}\}_{i,j=1,\dots,n}$ as the initial values for \mathbf{X} , \mathbf{V} , and $\{\delta_{ij}\}_{i,j=1,\dots,n}$. Moreover, from $\mathbf{X}^{(0)}$, one can compute the initial sum of squared residuals $SSR^{(0)}$ and the sample variance $\sigma^{2(0)} = SSR^{(0)}/m$,

which can be used as the initial value of σ^2 . In addition, the diagonal elements of the sample covariance matrix of $\mathbf{V}^{(0)}$ can be used as initial values for the λ_j 's.

At each iteration, we will first propose a new value of λ_j from its conditional posterior distribution given the other unknowns. From (5), the full conditional posterior distribution of λ_j is the Inverse Gamma distribution $IG(\alpha + n/2, \beta_j + s_j/2)$, where s_j/n is the sample variance of the j th coordinates of the \mathbf{v}_i 's. By Algorithm 1 described in Nagano *et al.* (2019), the transformation T from \mathbf{v}_i to \mathbf{x}_i is

$$\mathbf{x}_i = T(\mathbf{v}_i) = \cosh(\|\tilde{\mathbf{v}}_i\|_{\mathcal{L}}) \boldsymbol{\mu}_0^p + \sinh(\|\tilde{\mathbf{v}}_i\|_{\mathcal{L}}) \frac{\tilde{\mathbf{v}}_i}{\|\tilde{\mathbf{v}}_i\|_{\mathcal{L}}}, \quad (6)$$

where $\tilde{\mathbf{v}}_i = (0, \mathbf{v}_i) \in \mathbb{R}^{p+1}$ and $\|\tilde{\mathbf{v}}_i\|_{\mathcal{L}} \equiv \sqrt{\langle \tilde{\mathbf{v}}_i, \tilde{\mathbf{v}}_i \rangle_{\mathcal{L}}}$. Correspondingly, the inverse transformation T^{-1} from \mathbf{x}_i to \mathbf{v}_i is

$$\tilde{\mathbf{v}}_i = (0, \mathbf{v}_i) = T^{-1}(\mathbf{x}_i) = \frac{\operatorname{arccosh}(\alpha)}{\sqrt{\alpha^2 - 1}} (\mathbf{x}_i - \alpha \boldsymbol{\mu}_0^p), \quad (7)$$

where $\alpha = -\langle \boldsymbol{\mu}_0^p, \mathbf{x}_i \rangle_{\mathcal{L}}$. By transformation T , applying a Gaussian prior on $\mathbf{v}_i \in \mathbb{R}^p$ is then equivalent to using a hyperbolic wrapped normal prior on $\mathbf{x}_i \in \mathbb{H}^p(\kappa)$ with mean $\boldsymbol{\mu}_0^p = (1, 0, \dots, 0) \in \mathbb{R}^{p+1}$ and covariance matrix Λ .

With this transformation in mind, we then use a random walk Metropolis-Hasting algorithm to sample the \mathbf{v}_i 's and σ^2 . Since we specify a Gaussian prior on \mathbf{v}_i , we correspondingly use a normal proposal density. To choose the variance of the normal proposal density, we first write down the full conditional posterior density of \mathbf{v}_i , that is,

$$\pi(\mathbf{v}_i | \dots) \propto \exp \left[-\frac{1}{2} (Q_1 + Q_2) - \sum_{j \neq i, j=1}^n \log \Phi \left(\frac{\delta_{ij}}{\sigma} \right) \right], \quad (8)$$

where $Q_1 = \sum_{j \neq i, j=1}^n (\delta_{ij} - d_{ij})^2 / \sigma^2$ and $Q_2 = \mathbf{v}_i^\top \Lambda^{-1} \mathbf{v}_i$. From numerical experiments, we found that $\delta_{ij} = d_{\mathbb{H}^p(\kappa)}(T(\mathbf{v}_i), T(\mathbf{v}_j))$ is approximately of the order of $\sqrt{\kappa} \|\mathbf{v}_i\|$. Consequently, $(\delta_{ij} - d_{ij})^2$ can be approximated by a quadratic form of $\|\mathbf{v}_i\|$, so that Q_1 has $n - 1$ quadratic forms of $\|\mathbf{v}_i\|$ with coefficient $1/\sigma^2$, whereas $Q_2 = \mathbf{v}_i^\top \Lambda^{-1} \mathbf{v}_i$ has only one quadratic form of $\|\mathbf{v}_i\|$ with coefficient Λ . Thus, we conclude that Q_1 dominates the full conditional posterior distribution, and we may approximate the full conditional variance of \mathbf{v}_i by a constant multiple of $\sigma^2/(n - 1)$, which we use as the variance of the normal proposal density in the MCMC sampler.

Finally, from a preliminary numerical study similar to that carried out by Oh and Raftery (2001), we found that the full conditional density function of σ^2 can be well approximated by

the density function of $IG(m/2 + a, SSR/2 + b)$. Moreover, when the number of dissimilarities $m = n(n-1)/2$ is large, the Inverse Gamma density function can be well approximated by a normal density. Thus, we use a random walk Metropolis-Hasting algorithm with a normal proposal density and a variance proportional to the variance of $IG(m/2 + a, SSR/2 + b)$ to sample σ^2 .

We now summarize our MCMC algorithm. At iteration t :

1. For each $i = 1, \dots, p$, sample $\lambda_i^{(t)}$ as

$$\lambda_i^{(t)} \sim IG\left(\alpha + n/2, \beta_i + s_i^{(t-1)}/2\right),$$

where $s_i^{(t-1)}$ is the sample variance of the i th coordinates of $\mathbf{v}_i^{(t-1)}$ s.

2. For each $i = 1, \dots, n$, do the following:

- (a) Make a new proposal for $\mathbf{v}_i^{(t)}$ such that

$$\mathbf{v}_{i,\text{new}}^{(t)} \sim MVN_p\left(\mathbf{v}_i^{(t)}, \frac{c\sigma^{2(t-1)}}{n-1} \cdot I_p\right),$$

where I_p is the $p \times p$ identity matrix. In practice, we can simply set the constant multiple $c = 1$.

- (b) Set $\mathbf{v}_i^{(t)} = \mathbf{v}_{i,\text{new}}^{(t)}$ with probability

$$p = \min\left(1, \frac{\pi_{\mathbf{v}}(\mathbf{v}_{i,\text{new}}^{(t)})}{\pi_{\mathbf{v}}(\mathbf{v}_i^{(t)})}\right),$$

where $\pi_{\mathbf{v}}(\cdot)$ is the full conditional posterior density of \mathbf{v} in (8).

3. Make a new proposal for $\sigma^{2(t)}$ such that

$$\sigma_{\text{new}}^{2(t)} \sim N\left(\sigma^{2(t)}, \frac{c\gamma^{(t)}}{(\omega-1)^2(\omega-2)}\right),$$

where $\gamma^{(t)} = (SSR^{(t)}/2 + b)^2$ and $\omega = m/2 + a$. Set $\sigma^{2(t)} = \sigma_{\text{new}}^{2(t)}$ with probability

$$p = \min\left(1, \frac{\pi_{\sigma^2}(\sigma_{\text{new}}^{2(t)})}{\pi_{\sigma^2}(\sigma^{2(t)})}\right),$$

where $\pi_{\sigma^2}(\cdot)$ is the density function of $IG(m/2 + a, SSR^{(t)}/2 + b)$.

Using the above algorithm, we obtain samples from the full posterior density. The latent embeddings, \mathbf{X} , however are only indirectly involved in the posterior distribution through the dissimilarity measures, δ_{ij} . The posterior samples of \mathbf{X} , therefore, are invariant to isometric actions on $\mathbb{H}^p(\kappa)$. Thus in general, \mathbf{X} is not identifiable, and we can only recover the relative embedding of the objects instead of their absolute hyperbolic coordinates. [Oh and Raftery \(2001\)](#) suggested post-processing the MCMC samples of \mathbf{X} at each iteration of the MCMC via the Procrustes operation, so that the transformed \mathbf{X}' has sample mean 0 and a diagonal covariance matrix as specified in the prior. We found in simulations, however, that the MCMC algorithm mixed well without post-processing and returned accurate estimates of the model parameters. We therefore skipped this post-processing step, which has the added benefit of speeding up our algorithm, since the Procrustes transformation involves an eigen-decomposition of a large matrix.

Our solution is to estimate \mathbf{X} through the Bayesian estimates of the dissimilarities $\{\delta_{ij}\}$. To estimate $\{\delta_{ij}\}$, we observe that the likelihood in (3) dominates the posterior density in (5), and the term involving the SSR in (3) dominates the likelihood, so that the posterior mode of $\{\delta_{ij}\}$ can be well approximated by the posterior sample of $\{\delta_{ij}\}$ that minimizes the SSR. Moreover, the $\{\delta_{ij}\}$ that minimizes the SSR also minimize the MDS goodness-of-fit measure stress, as the stress is just the square root of SSR after normalization. We then define the Bayesian estimate of $\{\delta_{ij}\}$ as the posterior stress-minimizing estimate

$$\{\widehat{\delta}_{ij}\} \equiv \arg \min_{\{\delta_{ij}\}^{(t)}} SSR^{(t)} = \arg \min_{\{\delta_{ij}\}^{(t)}} \text{stress}^{(t)}, \quad (9)$$

where the superscript (t) indicates that the posterior sample is drawn from the t th MCMC iteration. Finally, since each $\{\delta_{ij}\}^{(t)}$ corresponds to a unique $\mathbf{X}^{(t)}$ from the posterior, we simply take the posterior sample of $\mathbf{X}^{(t)}$ corresponds to $\{\widehat{\delta}_{ij}\}$ as our Bayesian estimate of $\widehat{\mathbf{X}}$.

4.2 Case-control Likelihood Approximation

For dissimilarity data with a sample size of around $n < 200$, 20,000 iterations of the MCMC algorithm take about 300 seconds using a standard personal computer. However, since the proposal of \mathbf{v}_i involves calculations across n terms, and for each iteration we need to update \mathbf{v}_i n times in total, the time complexity of each iteration is approximately $O(n^2)$. When the sample size n increases, the algorithm quickly become computationally intractable.

We propose a stratified case-control log-likelihood to approximate the original posterior log-likelihood to facilitate computation using larger datasets. Our case-control approach is based on work by [Raftery *et al.* \(2012\)](#) for social networks, where they studied a posterior log-likelihood approximation of the latent space model described in [Hoff *et al.* \(2002\)](#). The core intuition is that, for each object i fixed, if we stratify all other objects regarding their dissimilarities to i , then there are many fewer objects that are similar to i than there are objects that are very dissimilar. This imbalance creates an opportunity to borrow ideas from the widely-used case-control technique from epidemiology. The samples in a case-control study can also be stratified into two distinct groups, where the “case” group has the outcome of interest, but is often rare and hard to collect compared to the “control” group.

This suggests that the statistical approximation technique in case-control studies can be used to approximate the posterior distribution of \mathbf{v}_i . If we view the similar objects to object i as samples in the case group, and the rest as being in the control group, we can approximate the posterior distribution using all the samples in the case group and a random sample from the control group. Moreover, to increase precision, we further stratify the samples in the control group by their dissimilarities to object i , and randomly sample from each stratum by their weight determined by their contributions to the proposal likelihood change to enhance the accuracy of the approximation. Under the proposed case-control stratification scheme, we accelerate the MCMC time complexity from $O(n^2)$ to $O(n)$.

We will now give details of the stratified case-control log-likelihood. The full conditional log-posterior density of \mathbf{v}_i is

$$l_i \equiv \log \pi(\mathbf{v}_i \mid \cdots) \propto - \sum_{j \neq i, j=1}^n \left[\frac{(\delta_{ij} - d_{ij})^2}{2\sigma^2} + \log \Phi \left(\frac{\delta_{ij}}{\sigma} \right) \right] - \frac{1}{2} \mathbf{v}_i^\top \Lambda^{-1} \mathbf{v}_i, \quad (10)$$

The first step is to divide object $j = 1, 2, \dots, n, j \neq i$ into M different strata $S_1^{(i)}, S_2^{(i)}, \dots, S_M^{(i)}$ according to their observed dissimilarities with respect to object i . The partition of the strata can be highly customized, as long as the total number of strata $M \ll n$. We will later describe several partition strategies in detail later in [Section 6.2](#) and [6.3](#). Given the strata, we can write the log-likelihood as

$$l_i = - \sum_{k=1}^M \sum_{j \in S_k^{(i)}} \left[\frac{(\delta_{ij} - d_{ij})^2}{2\sigma^2} + \log \Phi \left(\frac{\delta_{ij}}{\sigma} \right) \right] - \frac{1}{2} \mathbf{v}_i^\top \Lambda^{-1} \mathbf{v}_i = \sum_{k=1}^M l_{i,k} - \frac{1}{2} \mathbf{v}_i^\top \Lambda^{-1} \mathbf{v}_i. \quad (11)$$

where $l_{i,k} = -\sum_{j \in S_k^{(i)}} [(\delta_{ij} - d_{ij})^2 / 2\sigma^2 + \log \Phi(\delta_{ij}/\sigma)]$ is the likelihood contribution from stratum $S_k^{(i)}$.

If a stratum $S_k^{(i)}$ belongs in the case group, we will compute its log-likelihood explicitly. Otherwise, if $S_k^{(i)}$ belongs in the control group, we will randomly sample $n_{i,k}$ objects from the strata $S_k^{(i)}$ and estimate the strata's log-likelihood contribution by

$$\hat{l}_{i,k} = -\frac{N_{i,k}}{n_{i,k}} \sum_{j \in n_{i,k} \text{ samples}} \left[\frac{(\delta_{ij} - d_{ij})^2}{2\sigma^2} + \log \Phi \left(\frac{\delta_{ij}}{\sigma} \right) \right], \quad (12)$$

where $N_{i,k}$ is the number of elements in strata $S_k^{(i)}$. Since the estimator $\hat{l}_{i,k}$ is based on a random sample from the strata, we always have $\mathbb{E}(\hat{l}_{i,k}) = l_{i,k}$, so that the log-likelihood estimator is unbiased. For the sake of analysis, we now assume the first C strata are considered as cases, which we denote as $S_1^{(i)}, S_2^{(i)}, \dots, S_C^{(i)}$, and the rest are controls. Then, the stratified case-control approximate log-likelihood for object i becomes

$$\hat{l}_i = \sum_{k=1}^C l_{i,k} + \sum_{k=C+1}^M \hat{l}_{i,k} - \frac{1}{2} \mathbf{v}_i^\top \Lambda^{-1} \mathbf{v}_i. \quad (13)$$

where $l_{i,k}$ the $S_k^{(i)}$'s likelihood contribution in (11) and $\hat{l}_{i,k}$ are the log-likelihood estimators in (12).

We now describe how to determine the subsample size $n_{i,k}$. To accelerate the MCMC iteration to approximately $O(n)$, we want object i 's overall random sample size $n_i \equiv \sum_{k=1}^M n_{i,k} \ll n$. To do this, we pick a moderate control-to-case rate r , and let n_i be r times of the average number of objects in the case group. That is, we set $n_i \equiv r \cdot \frac{1}{n} \sum_{i=1}^n \sum_{k=1}^C |S_k^{(i)}|$, where $|S_k^{(i)}|$ denotes the number of objects in $S_k^{(i)}$. Given the fixed n_i , we assign $n_{i,k}$ proportional to the stratum $S_k^{(i)}$'s contribution to the log-likelihood change in sampling \mathbf{v}_i . We conduct the following pilot MCMC to determine the stratum $S_k^{(i)}$'s likelihood contributions. For object i fixed, we first draw a simple random sample over its control group with size n_i , and use them to construct an approximate log-likelihood

$$\tilde{l}_i \equiv \sum_{k=1}^C l_{i,k} + \frac{n - \sum_{k=1}^C |S_k^{(i)}|}{n_i} \sum_{j \in n_i \text{ samples}} \left[\frac{(\delta_{ij} - d_{ij})^2}{2\sigma^2} + \log \Phi \left(\frac{\delta_{ij}}{\sigma} \right) \right] - \frac{1}{2} \mathbf{v}_i^\top \Lambda^{-1} \mathbf{v}_i, \quad (14)$$

which we will use in the pilot MCMC. Once again, since we randomly sample from the population,

\tilde{l} is unbiased. Then, at each iteration t , we calculate the log-likelihood change for \mathbf{v}_i as

$$\begin{aligned}\Delta \tilde{l}_i^{(t)} &= \tilde{l}_i(\mathbf{v}_{i,\text{new}}^{(t)}) - \tilde{l}_i(\mathbf{v}_i^{(t)}) \\ &= \sum_{k=1}^C \left[l_{i,k}(\mathbf{v}_{i,\text{new}}^{(t)}) - l_{i,k}(\mathbf{v}_i^{(t)}) \right] + \sum_{k=C+1}^M \left[\tilde{l}_{i,k}(\mathbf{v}_{i,\text{new}}^{(t)}) - \tilde{l}_{i,k}(\mathbf{v}_i^{(t)}) \right] + \Delta_i \\ &= \sum_{k=1}^C \Delta l_{i,k} + \sum_{k=C+1}^M \Delta \tilde{l}_{i,k} + \Delta_i ,\end{aligned}$$

where $\Delta_i = -(\mathbf{v}_{i,\text{new}}^\top \Lambda^{-1} \mathbf{v}_{i,\text{new}} - \mathbf{v}_i^\top \Lambda^{-1} \mathbf{v}_i)/2$. We then define

$$w_{i,k}^{(t)} = \left| \frac{\Delta \tilde{l}_{i,k}}{\sum_{g=C+1}^M \Delta \tilde{l}_{i,g}} \right| \quad \text{for } k = C + 1, C + 2, \dots, M ,$$

and calculate the relative weights as

$$w_{i,k} = \frac{1}{T-1} \sum_{t=1}^{T-1} w_{i,k}^{(t)} ,$$

where T is the number of iterations in the pilot MCMC run after burn-in and thinning. Finally, we take the subsample size $n_{i,k}$ as

$$n_{i,k} = n_i \cdot \frac{w_{i,k}}{\sum_{g=C+1}^M w_{i,g}} ,$$

for $k = C + 1, \dots, M$. To summarize, the algorithm is as follows.

1. For each object $i = 1, \dots, n$, partition all other objects into M strata via a user-defined, dissimilarity-based strategy.
2. Set the strata defined with small dissimilarities $S_1^{(i)}, S_2^{(i)}, \dots, S_C^{(i)}$ as cases, and the rest as controls.
3. For each object i , randomly sample n_i objects from the control group.
4. Run a pilot MCMC with the approximate log-likelihood described in (14).
5. Record the relative weights $w_{i,k}$ and compute the subsample sizes $n_{i,k}$.
6. For each object $i = 1, 2, \dots, n$, sample $n_{i,k}$ objects from strata $S_k^{(i)}$ for $k = C + 1, C + 2, \dots, M$.

7. Run a full MCMC with the original log-likelihood functions l_1, l_2, \dots, l_n replaced by the stratified case control log-likelihood functions in (13).

In the following sections, we evaluate both of full and approximate strategies for sampling from the posterior using both simulated and observed data.

5 Simulation Experiments

We conducted simulation experiments to evaluate aspects of the proposed statistical model and algorithm. First, we evaluate BHMDs’s element-wise estimation performance for the true dissimilarities, δ_{ij} , and the measurement error variance, σ^2 . Then, we evaluate the overall estimation performance using the coverage rate of the posterior credible interval (CI) over all the $\{\delta_{ij}\}$. Lastly, we evaluate the robustness of the algorithm by examining its calibration under a variety of data generating distributions.

To evaluate BHMDs’s estimation performance, we wish to test it under different dataset sizes n , hyperbolic dimensions p , and noise levels σ . Throughout our experiments, we fix the hyperbolic curvature $\kappa = 1$, and generate the simulation data as follows:

1. For each combination of $(n, p) \in \{50, 100\} \times \{2, 5\}$, sample $\mathbf{X} = \{\mathbf{x}_1, \dots, \mathbf{x}_n\}$ from the hyperbolic wrapped normal distribution such that $\mathbf{x}_1, \dots, \mathbf{x}_n \sim_{i.i.d.} \mathcal{G}(\mathbf{0}_p, 3I_p)$, where $\mathcal{G}(\cdot, \cdot)$ is the distribution described in Nagano *et al.* (2019) and I_p is the p -dimensional identity matrix. Specifically, the wrapped normal distribution $\mathcal{G}(\cdot, \cdot)$ samples from a normal distribution on the tangent space at the hyperbolic origin in \mathbb{R}^p , projects the tangent space onto the hyperbolic space by the transportation described in (6), results in a Gaussian-like distribution on \mathbb{H}^p , and generates tree-like, hierarchical data.
2. Compute the true dissimilarities $\{\delta_{ij}\}_{i,j=1,\dots,n} = d_{\mathbb{H}^p(1)}(\mathbf{x}_i, \mathbf{x}_j)$. Then, for each $\sigma \in \{1, 1.5, 2\}$, generate the corresponding observed dissimilarity matrices $\{d_{ij}\}_{i,j=1,\dots,n}$, with entries d_{ij} drawn from (3).
3. Apply the full BHMDs MCMC to the $\{d_{ij}\}$ ’s and record the approximate posterior mode estimates $\{\hat{\delta}_{ij}\}$ described in (9), posterior mean $\hat{\sigma}$, and the matrix-wise converge rate

$$C \equiv \frac{\sum_{i < j} I\left(\delta_{ij} \in \left[q_{ij}^{(\alpha/2)}, q_{ij}^{(1-\alpha/2)}\right]\right)}{m}, \quad (15)$$

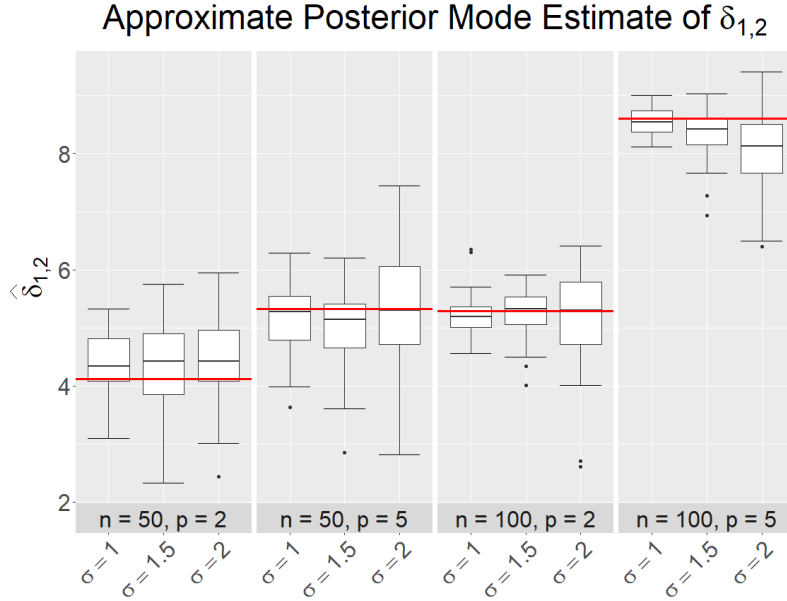


Figure 1: Simulation results of the BHMDs estimation performance on the true dissimilarity $\delta_{1,2}$. The facet labels, i.e., $n = 50, p = 2$, correspond to the sample size n and hyperbolic dimension p of the true dissimilarity data, with $(n, p) \in \{50, 100\} \times \{2, 5\}$. The x-axis labels, i.e. $\sigma = 1$, correspond to the noise level of the observed dissimilarity data, with $\sigma \in \{1, 1.5, 2\}$. For each level of (n, p) , we generate a true dissimilarity matrix $\{\delta_{ij}\}$. Then, for each level of σ , we generate 50 sets of noisy dissimilarity matrix $\{d_{ij}\}$ for each $\{\delta_{ij}\}$. We use the proposed BHMDs algorithm to estimate $\{\delta_{ij}\}$. Without loss of generality, we summarized the results on $\hat{\delta}_{1,2}$, the approximate posterior mode estimate of the dissimilarity between object 1 and 2, in the box plots above. Each box plot corresponds to 50 estimates of $\hat{\delta}_{1,2}$ at a level of (n, p, σ) , and red lines in each facet correspond to the true dissimilarity measures $\delta_{1,2}$ at level (n, p) . All box plots closely center around the true values, indicating BHMDs precisely and robustly predicts the true dissimilarity measure.

where $(q_{ij}^{(\alpha/2)}, q_{ij}^{(1-\alpha/2)})$ are the $(\alpha/2)$ and $(1 - \alpha/2)$ quantiles of the posterior samples of δ_{ij} and $m = n(n - 1)/2$.

We plot the simulation results on $\{\hat{\delta}_{ij}\}$, $\hat{\sigma}$, and coverage rate in Figure 1, 2, and 3 respectively. For any combination of (n, p, σ) , all the boxplots are concentrated tightly around the red horizontal lines representing the true values in all three plots, indicating that BHMDs obtains precise and robust estimates of δ_{ij} , σ^2 , and close to the nominal coverage rate.

We are interested in further testing the robustness of the BHMDs algorithm using dissimilarity data generated via different distributions defined with a variety of dimensions, curvatures, and distribution parameters. For this we use marginal calibration, a criterion which comprehensively assesses the predictive performance of the forecasting distribution. Suppose at times or instances

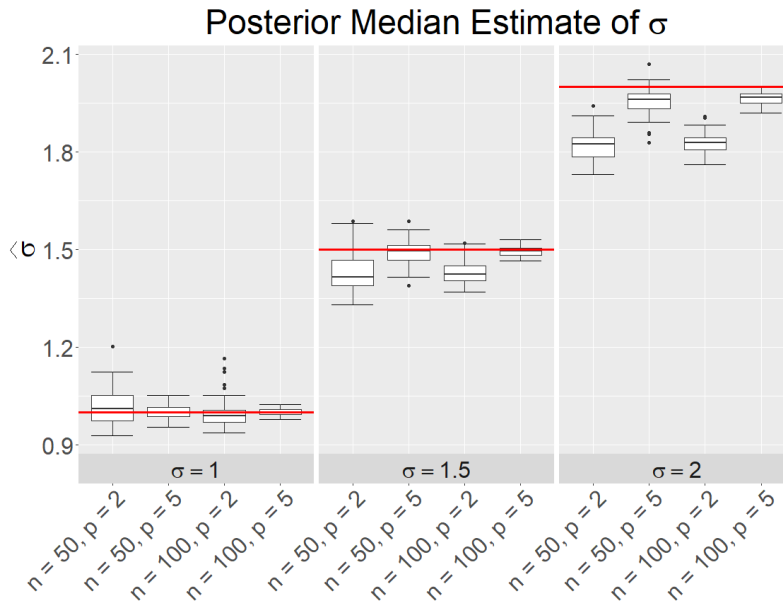


Figure 2: Simulation result of the BHMDs estimation performance on the true measurement error σ . The facet labels, i.e. $\sigma = 1$, correspond to the noise level of the observed dissimilarity data, with $\sigma \in \{1, 1.5, 2\}$. The x-axis labels, i.e., $n = 50, p = 2$, correspond to the sample size n and hyperbolic dimension p of the true dissimilarity data, with $(n, p) \in \{50, 100\} \times \{2, 5\}$. At each level of (n, p, σ) , we generate 50 sets of noisy observations of the true dissimilarity matrix, and use the proposed BHMDs algorithm to estimate σ . We summarized the results on $\hat{\sigma}$, the posterior mean estimate of σ , in the box plots above. Each box plot corresponds to 50 estimates of $\hat{\sigma}$ at a level of (n, p, σ) , and red lines in each facet correspond to the true noise level σ value. We see that as the noise level increases, the accuracy of the estimator $\hat{\sigma}$ decreases, though the difference $|\hat{\sigma} - \sigma|$ decreases as the sample size n increases. In general, all box plots closely center around the true values, indicating BHMDs precisely and robustly measures the amount of uncertainty in data.

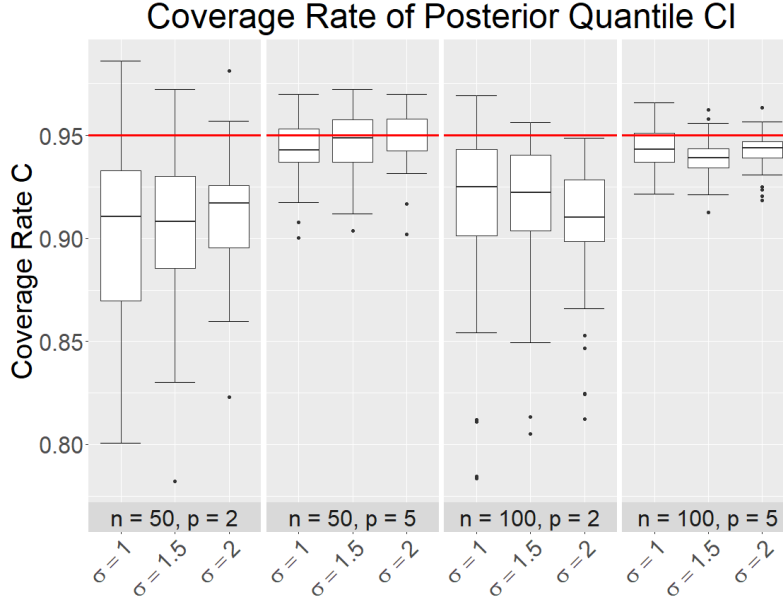


Figure 3: Simulation result of the BHMDS credible interval’s coverage performance. The facet labels, i.e., $n = 50, p = 2$, correspond to the sample size n and hyperbolic dimension p of the true dissimilarity data, with $(n, p) \in \{50, 100\} \times \{2, 5\}$. The x-axis labels, i.e. $\sigma = 1$, correspond to the noise level of the observed dissimilarity data, with $\sigma \in \{1, 1.5, 2\}$. At each level of (n, p, σ) , we generate 50 sets of noisy observations of the true dissimilarity matrix, and use the proposed BHMDS algorithm to estimate and record the posterior samples of $\{\delta_{ij}\}$. Each box plot contains 50 matrix-wise coverage rates corresponding to the 50 noisy observations, calculated as described in (15). The red lines in each facet correspond to the nominal 95% coverage rate. We can observe that BHMDS achieves close-to-nominal coverage rates at all levels of (n, p, σ) , and the coverage improves as the sample size n increases.

$s = 1, 2, \dots, S$, nature picks distributions G_1, G_2, \dots, G_S , and we predict them with forecasting distributions F_1, F_2, \dots, F_S . We further let x_1, x_2, \dots, x_S be observations randomly sampled from G_1, G_2, \dots, G_S at time $1, 2, \dots, S$. We define $\{F_s\}_{s=1,2,\dots,S}$ as marginally calibrated with respect to $\{G_s\}_{s=1,2,\dots,S}$ if

$$\bar{G}(x) = \lim_{S \rightarrow \infty} \left\{ \frac{1}{S} \sum_{s=1}^S G_s(x) \right\} \quad \text{and} \quad \bar{F}(x) = \lim_{S \rightarrow \infty} \left\{ \frac{1}{S} \sum_{s=1}^S F_s(x) \right\} \quad (16)$$

exist and equal to each other for all x . In practice, we cannot access G_s , but we can always access the empirical cumulative distribution function (CDF) of the observations. Specifically, Theorem 3 of [Gneiting *et al.* \(2007\)](#) shows that for continuous, strictly increasing G_s and F_s 's, $\{F_s\}_{s=1,2,\dots,S}$ is marginally calibrated with respect to $\{G_s\}_{s=1,2,\dots,S}$ if and only if

$$\hat{G}_S(x) = \frac{1}{S} \sum_{s=1}^S \mathbf{1}(x_s \leq x) \rightarrow \bar{F}(x) \quad \text{almost surely for all } x, \quad (17)$$

so that the empirical CDF of the observations converges almost surely to the average predictive CDF. [Gneiting *et al.* \(2007\)](#) suggested plotting the difference between $\hat{F}_S(x) = \frac{1}{S} \sum_{s=1}^S F_s(x)$ and $\hat{G}_S(x)$ over all x to assess the marginal calibrations of the forecasting distributions, so that the smaller the difference in the plot, the better the calibration.

To evaluate the estimation performance of BHMDs via marginal calibration, we need to first specify the distributions $\{G_s\}_{s=1,2,\dots,S}$ and $\{F_s\}_{s=1,2,\dots,S}$. We cannot choose the wrapped normal distribution $\mathcal{G}_s(\mathbf{x})$ as G_s , since G_s is required to be univariate, yet $\mathcal{G}_s(\mathbf{x})$ is a function of the multivariate random variable \mathbf{x} , which we wish to vary under different hyperbolic dimensions. Thus alternatively, we choose the distribution of δ_{ij} as G_s , which is the distribution of the hyperbolic distance between coordinates \mathbf{x}_i and \mathbf{x}_j randomly sampled from a given $\mathcal{G}_s(\mathbf{x})$, and choose the F_s as the distribution of $\hat{\delta}_{ij}$ estimated by BHMDs. Choosing a distribution such as G_s is beneficial, as it is inherently univariate and is uniquely determined by the data generating distribution $\mathcal{G}_s(\mathbf{x})$, so that if BHMDs estimates the true dissimilarity well, the distribution of $\hat{\delta}_{ij}$ will resemble the distribution of δ_{ij} . Given G_s 's and F_s 's, for each $s = 1, 2, \dots, 1000$, we randomly generate the

parameters

$$\begin{aligned}
p^{(s)} &\sim \text{Multinomial}(2, 3, 4, 5) \text{ with equal probability ,} \\
\kappa^{(s)} &\sim \text{Unif}(0.2, 2) , \\
\mu_p^{(s)} &\sim \mathcal{N}_p(0, 2I_p) , \\
\Sigma_{ii}^{(s)} &\sim_{i.i.d.} \text{Unif}(5, 10), \text{ and } \Sigma_{ij}^{(s)} = 0 \text{ for all } i, j = 1, 2, \dots, p, i \neq j .
\end{aligned}$$

For each set of parameters, we sample 20 sets of $\mathbf{V}_1^{(s)}, \mathbf{V}_2^{(s)}, \dots, \mathbf{V}_{20}^{(s)} \sim \mathcal{N}_p(\mu_p^{(s)}, \Sigma^{(s)})$, each of size $n = 50$, and transform them into hyperbolic coordinates $\mathbf{X}_1^{(s)}, \mathbf{X}_2^{(s)}, \dots, \mathbf{X}_{20}^{(s)}$ by the transformation in (6). From the coordinates, we compute the true dissimilarity matrices and generate their noisy observations at noise level $\sigma = 1$. We then apply BHMDs to the noisy matrices and record the estimated dissimilarities $\{\widehat{\delta}_{ij}\}_1^{(s)}, \{\widehat{\delta}_{ij}\}_2^{(s)}, \dots, \{\widehat{\delta}_{ij}\}_{20}^{(s)}, i, j = 1, 2, \dots, n$.

Given the distributions G_s at each instance s , we can sample x_1, x_2, \dots, x_S explicitly and use them to construct $\widehat{G}_S(x)$. On the other hand, we cannot directly access the F_s 's, but we can estimate them by the empirical CDFs \widetilde{F}_s 's from the posterior estimates. To minimize the correlation between the samples, we use the samples $\{\widehat{\delta}_{i,i+1}\}_1^{(s)}, \{\widehat{\delta}_{i,i+1}\}_2^{(s)}, \dots, \{\widehat{\delta}_{i,i+1}\}_{20}^{(s)}$ for $i = 1, 2, \dots, n - 1$ to compute \widetilde{F}_s 's. Finally, we plot the difference

$$\frac{1}{S} \sum_{s=1}^S \widetilde{F}_s(x) - \widehat{G}_S(x) \tag{18}$$

in Figure 4 in red. We further evaluate the marginal calibration of the Euclidean `bmds` via the same process and plot the difference in blue. The BHMDs method is much more calibrated than the `bmds` method, as the calibration curve for the BHMDs method is closer to zero for all threshold values on the x -axis. This suggests when the dissimilarity data is hierarchical, tree-like, or has intrinsic hyperbolic property, the proposed BHMDs algorithm yields much more precise estimates of the true dissimilarity compared to Euclidean MDS method.

6 Data Analysis

We now apply the proposed BHMDs algorithm to analyze a variety of dissimilarity datasets. First, we cross-compare BHMDs with multiple prevalent MDS algorithms using MDS goodness-of-fit criteria with respect to several hierarchical dissimilarity data collected in social network and

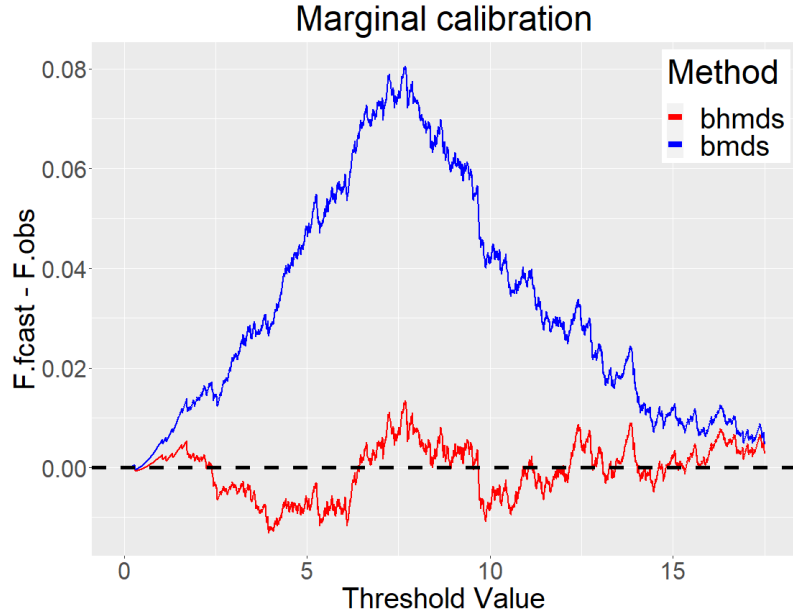


Figure 4: The marginal calibration result for BHMDs and `bmds`. The x-axis corresponds to the threshold values of the dissimilarity distribution. The y-axis corresponds to the difference as described in (18). The red line corresponds to the marginal calibration plot of BHMDs, the blue line corresponds to the marginal calibration plot of `bmds`, and the black horizontal dashed line corresponds to $y = 0$. We can observe that, when the true dissimilarity are generated from the hyperbolic geometry, BHMDs performs significantly better than `bmds`, with the difference only fluctuating in a small interval around zero, in contrast to the `bmds` difference, where there is a large spike at $x = 7.5$. This suggests that BHMDs outperforms `bmds` in estimating dissimilarities when the data is hierarchical.

Natural Language Processing (NLP) studies. Then, we present a case study of the case-control likelihood approximation on a hierarchical NLP hypernym data. Lastly, we apply BHMDs with a global human gene expression data to investigate the cellular differentiation of different cell types with confidence quantification on their rank statistics.

6.1 Comparison with Existing MDS Approaches

In this section, we apply BHMDs algorithm to several tree-like, hierarchical datasets and evaluate its embedding performance via MDS goodness-of-fit criteria stress and distortion.

We first give the definitions of the MDS goodness-of-fit criteria. Stress is one of the most prevalent criteria in the MDS literature, which measures the L_2 goodness-of-fit of the embedding. Given the observed dissimilarities $\{d_{ij}\}$ and its MDS embedding $\{\widehat{\delta}_{ij}\}$, their stress is defined as

$$\text{stress} \left(\{d_{ij}\}, \{\widehat{\delta}_{ij}\} \right) \equiv \sqrt{\frac{\sum_{i<j} (d_{ij} - \widehat{\delta}_{ij})^2}{\sum_{i<j} d_{ij}^2}}, \quad i, j = 1, \dots, n. \quad (19)$$

The distortion, on the other hand, measures the L_1 goodness-of-fit of the embedding, defined as

$$\text{Distortion} \left(\{d_{ij}\}, \{\widehat{\delta}_{ij}\} \right) \equiv \frac{1}{m} \sum_{i<j} \frac{|d_{ij} - \widehat{\delta}_{ij}|}{d_{ij}}, \quad i, j = 1, \dots, n, \quad (20)$$

where $m = n(n-1)/2$ is the number of dissimilarities. Both criteria normalize the difference terms by the observed dissimilarities, which enables cross-comparison among datasets with different size and scale.

We consider the following datasets in our numerical study. We first consider the Zachary’s Karate Club dataset, a commonly used social network of a university karate club, first described by [Zachary \(1976\)](#) and studied via the hyperbolic MDS algorithms `hydra` and `hydraPlus` in [Keller-Ressel and Nargang \(2020\)](#). Next, we consider a phylogenetic tree dataset which expresses the genetic heritage of mosses growing in urban environments, first described in [Hofbauer *et al.* \(2016\)](#) and studied in [De Sa *et al.* \(2018\)](#). We further consider two tree-like, hierarchical datasets: one is a Computer Science Ph.D. advisor-advisee network, available from [Doreian \(2006\)](#) and also studied in [De Sa *et al.* \(2018\)](#); the other is the WordNet mammals subtree dataset, a NLP hypernym dataset studied in [Nickel and Kiela \(2017\)](#). All of the four datasets come in the form of undirected graphs, thus we take the shortest path lengths on the graph between objects i and

Table 1: Embedding performance of the four datasets in terms of the stress criteria. The red text correspond to the optimal stress values, and the blue text correspond to the second optimal values. We can observe that, the stress-minimizing hyperbolic MDS methods, namely BHMDs and `hydraPlus`, constantly outperforms all other methods, and their embedding results are comparable. This indicates that tree-like, hierarchical data is best represented on hyperbolic geometry in terms of stress. Moreover, it shows that the BHMDs algorithm can be used to optimize the minimal-stress embedding.

	Size n	BHMDs	<code>hydraPlus</code>	<code>hydra</code>	<code>bmds</code>	<code>smacof</code>	<code>cmds</code>
Karate ($\kappa = 1$)	34	0.1780	0.1727	0.2105	0.2050	0.2112	0.2850
Phylo ($\kappa = 0.14$)	344	0.0413	0.0413	0.2091	0.1601	0.1594	0.2481
CS phd ($\kappa = 0.55$)	1025	0.1469	0.1471	0.2029	0.2281	0.2351	0.3862
Wordnet ($\kappa = 2.06$)	1141	0.0798	0.0807	0.1279	0.2722	0.2725	0.4928

j as the observed dissimilarity measures $\{d_{ij}\}$. Given the observed dissimilarity matrices, we fix the hyperbolic dimension as $p = 2$ and estimate their curvature κ 's as described in Appendix B, except for the karate dataset, where we set $\kappa = 1$ as in Keller-Ressel and Nargang (2020). Given the hyperbolic curvature and dimension, we use our BHMDs algorithm to compute the posterior estimate $\{\widehat{\delta}_{ij}\}$ and the corresponding goodness-of-fit criteria. To compare the embedding performance with existing methods, we included results from common hyperbolic MDS methods using the same hyperbolic curvature and dimension, as well as Euclidean MDS methods with dimension $p = 2$. The embedding results are displayed in Table 1 and 2. We can conclude from the tables that the BHMDs algorithm attains optimal or close-to-optimal embedding in terms of both criteria on all of the four datasets. This indicates that, when the dissimilarity data is tree-like or hierarchical, the proposed BHMDs algorithm not only quantifies the uncertainty in the observed dissimilarity data, but also embeds it into hyperbolic geometry with minimal information loss compared to the state-of-the-art MDS algorithms.

6.2 Approximated Log-likelihood: A Case Study

In this section, we present a case study to exemplify how to apply the stratified case-control log-likelihood and to evaluate the algorithm's likelihood precision and computational efficiency. We consider the WordNet mammals subtree dataset, a hierarchical NLP hypernym dataset studied in Nickel and Kiela (2017), as the input dataset. The WordNet dataset comes in as an undirected

Table 2: Embedding performance of the four datasets in terms of the Distortion criteria. The red text correspond to the optimal Distortion values, and the blue text correspond to the second optimal values. Again, we can observe that, the stress-minimizing hyperbolic MDS methods, namely BHMDs and `hydraPlus`, constantly outperforms all other methods even though they are not designed to optimize the Distortion, and their embedding results are comparable. This indicates that tree-like, hierarchical data is also best represented on hyperbolic geometry in terms of Distortion. Moreover, it shows that the BHMDs algorithm can be used to optimize the minimal-distortion embedding.

	Size n	BHMDs	<code>hydraPlus</code>	<code>hydra</code>	<code>bmds</code>	<code>smacof</code>	<code>cmds</code>
Karate ($\kappa = 1$)	34	0.3485	0.3287	0.4278	0.3986	0.3742	0.5234
Phylo ($\kappa = 0.14$)	344	0.1214	0.1206	0.6806	0.3552	0.3516	0.5918
CS phd ($\kappa = 0.55$)	1025	0.2869	0.2868	0.4545	0.4523	0.4510	0.7513
Wordnet ($\kappa = 2.06$)	1141	0.1441	0.1460	0.2242	0.4994	0.4967	0.9670

graph with $n = 1141$ nodes, and we take the shortest path lengths on the graph between objects i and j as the observed dissimilarities d_{ij} . We set the hyperbolic dimension $p = 2$ and estimate the curvature using the methods described in Appendix B.

We now explain how to apply the approximated log-likelihood to the WordNet dataset. For each object i , we first partition objects $j \in \{1, 2, \dots, n, j \neq i\}$ by their observed dissimilarity d_{ij} 's. Since we are using the shortest path length as dissimilarity, all d_{ij} 's are positive integers ranging from $1, 2, \dots, \max_j(d_{ij})$ for each i , and objects with the same d_{ij} value are in the same group. That is, we set

$$S_k^{(i)} \equiv \{\text{Object } j : d_{ij} = k, j = 1, 2, \dots, n, j \neq i\}, \quad k = 1, 2, \dots, \max_j(d_{ij}), \quad (21)$$

so that we collect all objects of distance k to object i in $S_k^{(i)}$.

We consider $S_1^{(i)}$ and $S_2^{(i)}$, the two strata defined with the smallest dissimilarities (neighbours and second-neighbours) as cases and all other $S_j^{(i)}$ for $j > 2$ as controls. We choose a control-to-case rate $r = 5$, so that in the approximated log-likelihood, we explicitly calculate over 7% of the terms in the original one. We run a pilot MCMC with 3000 iterations and 1000 burn-ins to compute the relative weights and samples sizes for each $S_j^{(i)}$ for $j > 2$. We then run the case control approximated log-likelihood MCMC to obtain the posterior estimate $\{\delta_{ij}\}$.

We first evaluate the overall estimation performance of the case-control MCMC algorithm in

term of the stress and computation time. We will run both the approximate and full MCMC algorithm with the WordNet dataset, and record the stress value of their posterior estimates as well as the computational times per 100 MCMC iterations. We display the results in Table 3 below. We observe that the case-control approximate log-likelihood MCMC achieves a comparable stress to the full MCMC but with only half of the computation time, indicating the approximate MCMC achieves fast and accurate estimates of the true dissimilarities for large datasets.

To evaluate the precision of the case-control likelihood, we compare the case-control log-likelihood change to the full log-likelihood change in the MCMC proposal of \mathbf{v}_i . If the case-control log-likelihood change approximates the full log-likelihood change well, the case-control MCMC will accept or reject in a similar pattern as the full MCMC. Recall that the change in the log likelihood, as defined in Section 4.2, is $\Delta\tilde{l}_i^{(t)} = \tilde{l}_i(\mathbf{v}_{i,\text{new}}^{(t)}) - \tilde{l}_i(\mathbf{v}_i^{(t)})$. For a valid comparison, it is essential to evaluate both likelihood changes with respect to the same \mathbf{v}_i proposal and parameters such as $\{\delta_{ij}\}, \sigma^2, \Lambda, \beta$. To this end, we first run the full MCMC algorithm with the Wordnet dataset, and record 100 sets of parameters $\boldsymbol{\theta}^{(i)} = (\{\delta_{ij}\}^{(i)}, (\sigma^2)^{(i)}, \Lambda^{(i)}, \beta^{(i)})$ from 100 MCMC iterations. For computational efficiency, we randomly sample 100 objects from the $n = 1141$ samples for each $\boldsymbol{\theta}^{(i)}$, and make proposal upon the corresponding $\mathbf{v}_1^{(i)}, \mathbf{v}_2^{(i)}, \dots, \mathbf{v}_{100}^{(i)}$ under $\boldsymbol{\theta}^{(i)}$. We compute the approximate likelihood change and the full likelihood change for each proposal $\mathbf{v}_j^{(i)}, i, j = 1, \dots, 100$, and plot the approximated log-likelihood change values against the full log-likelihood change values in Figure 5. We observe that the approximate log-likelihood change tightly aligned around $y = x$, with a strongly positive correlation $\rho = 0.82$. This indicates the log-likelihood values computed from the proposed case-control MCMC algorithm are a good approximation to the true log-likelihood values. Furthermore, the case-control MCMC shares a similar accept/reject pattern as the full MCMC and is able to properly sample from the posterior.

6.3 Quantifying Uncertainty in Human Gene Expression Data

We now use the proposed BHMDs algorithm to analyze a global human gene expression dataset. Lukk *et al.* (2010) integrated microarray data from 5372 human samples representing 369 different cells and tissue types, disease state and cell lines and constructed a global human gene expression map. The original data come in the form of a jointly normalized gene expression matrix of over 22000 probes sets times 5372 genes of 15 human cell types. To construct the dissimilarity

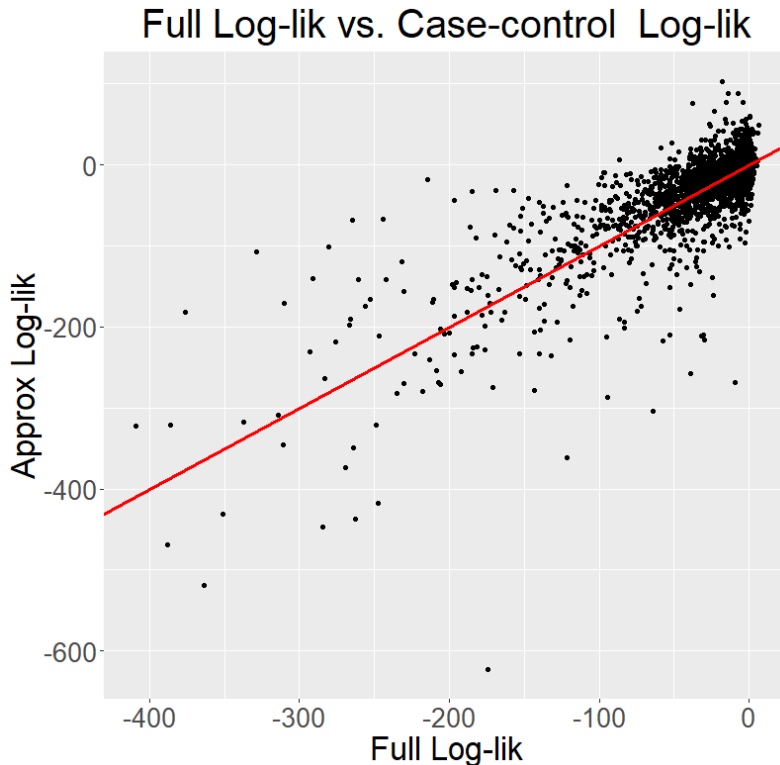


Figure 5: X-axis: Log-likelihood change values calculated via the full MCMC algorithm. Y-axis: Log-likelihood values calculated via the case-control approximate MCMC algorithm. The red line corresponds to the line $y = x$. We can observe that, the approximated log-likelihood changes tightly aligned around $y = x$ against the full log-likelihood changes, with a strongly positive correlation $\rho = 0.82$. This indicates the log-likelihood values computed from the proposed case-control MCMC algorithm is a good approximation of the true log-likelihood values, and the case-control MCMC share a similar accept/reject pattern as the full MCMC.

Table 3: Stress values and computational time per 100 MCMC iterations of the WordNet mammal subtree dataset with `hydraPlus`, approximated MCMC, and full MCMC. We can observe that, the approximated case-control algorithm achieves a comparable stress with `hydraPlus` and the full MCMC, indicating it estimates a close-to-optimal hyperbolic embedding of the WordNet dataset. More importantly, the proposed case-control algorithm is approximately twice as fast as the full MCMC algorithm. This will enable the BHMDs framework scalable with dissimilarity data of large sample sizes.

Method	hydraPlus	Approx	Full
Stress	0.081	0.085	0.080
MCMC time (100 iters)	-	28.39s	54.88s

matrix, the pairwise Euclidean distances of the gene vectors are taken, which results in a dissimilarity matrix with $n = 5372$. Although the dissimilarities are computed from a Euclidean embedding, [Zhou and Sharpee \(2021\)](#) proposed that the intrinsic geometry of the human gene expression data is hyperbolic. Moreover, [Elowitz *et al.* \(2002\)](#), [Oleksiak *et al.* \(2002\)](#), and [Raj and Oudenaarden \(2008\)](#) argued that the gene expression data is likely to contain measurement error. Thus, it is reasonable to apply the proposed BHMDs algorithm with the human gene expression dissimilarity matrix to quantify the uncertainty in analysis. Specifically, we use the case-control approximate MCMC algorithm to compute the Bayesian estimate of the cluster distances between cell type communities, and quantify the uncertainty on the rank statistics of cell types’ evolution pseudotimes.

We first elaborate the implementation details of the case-control approximated MCMC. As the dissimilarity matrix is computed from high dimensional Euclidean metrics, the original human gene expression dissimilarities are large, which leads to overflow issues. Thus, we preprocess the dissimilarity data as follows. We fix the hyperbolic curvature $\kappa = 1$, scale the dissimilarity matrix by a constant, and use `hydraPlus` to compute the corresponding stress with the hyperbolic dimension $p = 5$ as chosen in [Zhou and Sharpee \(2021\)](#). We repeat the above process with a grid search over the scaling constants, until we find an optimal constant. Such a process is similar in spirit to the algorithm described in Section B, as altering the curvature is roughly equivalent to scaling the distance as observed in (1), with the relationships between the dissimilarities unchanged. We found that scaling the dissimilarity by 10 yields the optimal stress at 0.046, resulting a rescaled matrix with an average dissimilarity at 15.12. Since the gene expression dissimilarity is continuous, we partition the rescaled dissimilarity by continuous intervals $[0, 7)$, $[7, 8)$, $[8, 9)$, \dots , $[24, \infty)$, and consider the dissimilarities that falls within $[0, 7)$ as in the case group. We further choose $r = 10$, so that we will explicitly compute 6% of the likelihood terms.

To compute the Bayesian estimate of the cell type cluster distance, at each MCMC iteration t , we record the cluster distance for cell type community C_i and C_j of size n_i and n_j as

$$d_{\text{cluster}}(C_i, C_j) = \frac{1}{n_i n_j} \sum_{(k,l) \in (C_i, C_j)} d_{\mathbb{H}}(\mathbf{x}_k, \mathbf{x}_l), \quad i \neq j, \quad i, j = 1, 2, \dots, 15, \quad (22)$$

where the community membership is given in the original data. We then take the posterior median of each $d_{\text{cluster}}(C_i, C_j)$, $i, j = 1, \dots, 15$, and plot them on Figure 6. Our Bayesian estimate identifies that the hematopoietic cells are distinct from all other cells, which is also observed in [Lukk *et al.*](#)

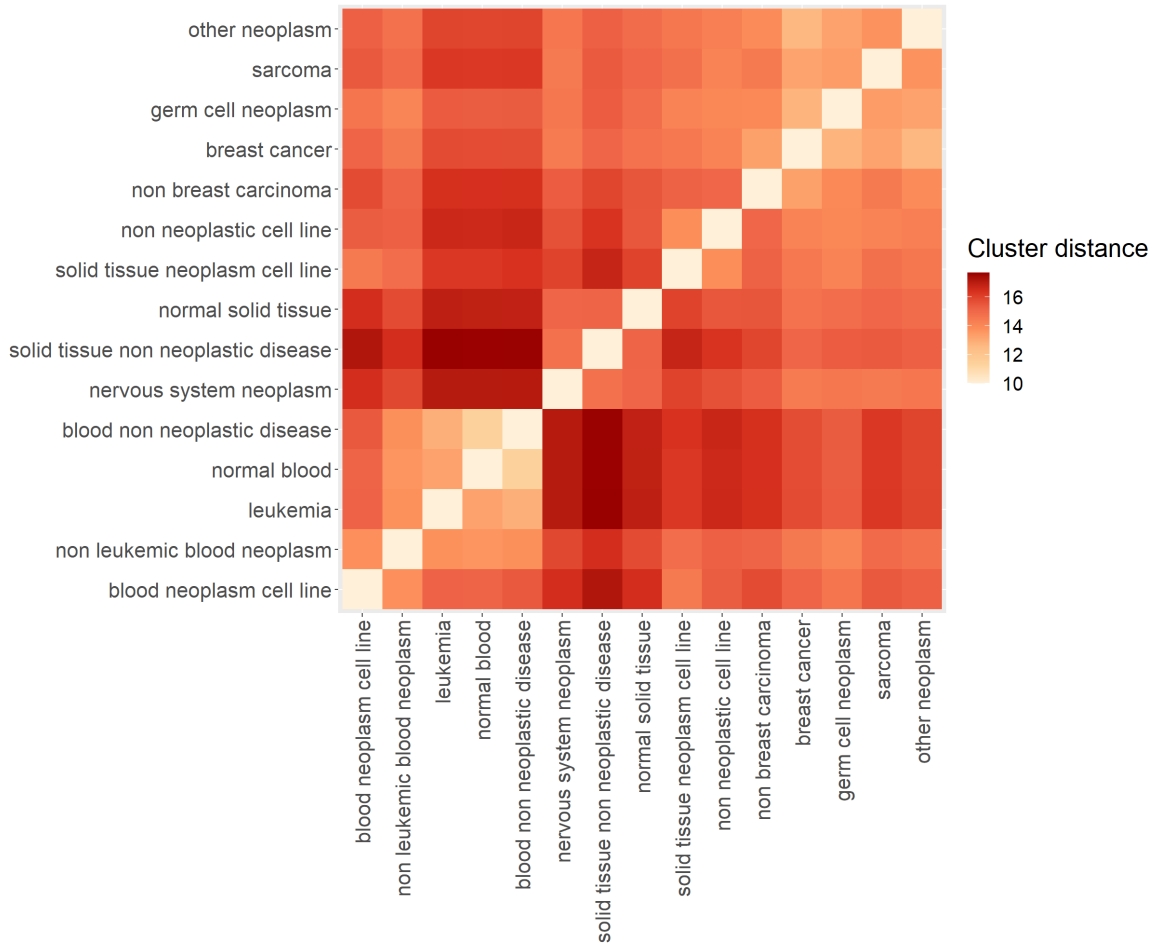


Figure 6: Heatmap of the cluster distance between cell type communities defined in (22). We observe the hematopoietic cells types, i.e., blood neoplasm cell line, non leukemic blood neoplasm, leukemia, normal blood, and blood non neoplastic disease, are distinct with all other cells. We also observed modularity in neoplasm cells, i.e. the clustering of breast cancer cell, germ cell neoplasm, sarcoma, and other neoplasm cells.

(2010). We also observe modularity in the neoplasm cells at the upper right corner of Heatmap 6, indicating their proximity in terms of evolutionary distance.

We further used the BHMDs algorithm to measure different cell types' cellular differentiation using rank statistics with uncertainty quantification, a feature that is not available from previous methods used to analyze these data. Cellular differentiation refers to the transition of immature cells into specialized types, which is a central task in modern developmental biology (Klimovskaia *et al.*, 2020). Specifically, Klimovskaia *et al.* (2020) studied the hierarchy of the single-cell data on hyperbolic geometry. For cells that are less differentiated, or at the beginning of a developmental process, they will be at the root of the evolutionary hierarchy and have relatively equal and small

distances with all other cells, so that by the nature of the hyperbolic geometry, they are more likely to be embedded around the hyperbolic origin. Similarly, for cells that are more differentiated, they will have relatively large distances with all other cells, so that they are more likely to be embedded distant from the origin. Thus, [Klimovskaia *et al.* \(2020\)](#) proposed that the hyperbolic distance between the origin and the cell’s embedded coordinate can be a good measure on the extent of the cell’s cellular differentiation, which they denoted as hyperbolic evolution pseudotime. In our study, at each iteration of the MCMC, we record the evolution pseudotime for each gene, and use them to construct the posterior credible intervals of the evolution pseudotime for each gene. To visualize the average evolution pseudotime for each cell type, we summarized the ranks statistics of each cell type as follows. For each cell type community, we randomly sample one of its gene, and draw from its nominal pseudotime confidence interval based on the posterior. Then, we rank the pseudotime drawn from each cell type community and record their rank statistics. We repeat the above process for 10,000 times. We then summarize the rank statistics by frequency in [Figure 7](#), where the ij th entry of the heatmap represents for the frequency of cell type i being the j th closest to the hyperbolic origin, which indicates it is j th less differentiated. [Figure 7](#) indicates that cell types within the same cluster in [Figure 6](#) share similar hierarchy, as the neoplasm cells obtain higher frequency for the higher rank statistics thus are less differentiated, whereas the hematopoietic cells obtain higher frequency for the lower rank statistics thus are more differentiated. Additionally, we observe that the germ cell neoplasm has the smallest evolution pseudotime, which to our knowledge is the first in literature, entailed by breast cancer cell, which is also argued in [Zhou and Sharpee \(2021\)](#) and [Friedmann-Morvinski and Verma \(2014\)](#). These results further shed light on the study of cancer stem cells, as short evolution pseudotimes of the two neoplasm cells suggests they are likely to be more de-differentiated, a hallmark often observed in malignant tumors.

7 Conclusion

In this work, we proposed a Bayesian approach to multidimensional scaling in hyperbolic space. Using a previously studied generating process for observed dissimilarities from [Oh and Raftery \(2001\)](#), we used prior distributions on hyperbolic space to derive the posterior distribution of the model parameters. We then proposed an MCMC procedure to sample from this posterior and also proposed a quick case-control method to efficiently sample from the posterior when the

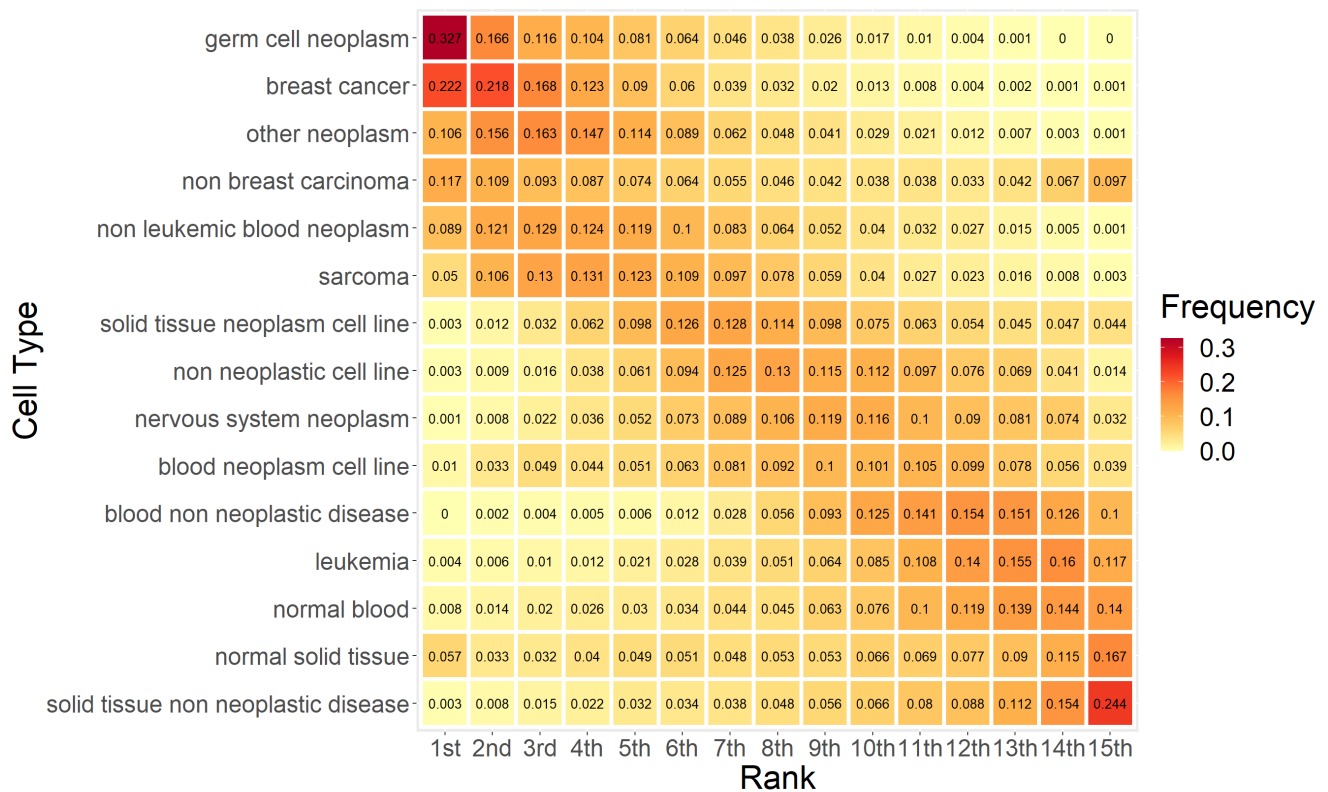


Figure 7: Heatmap on the frequency of the rank statistics for 15 different human cell type. We observe that cell types within the same cluster (hematopoietic, neoplasm) share similar hierarchy, with the neoplasm cell on the higher hierarchy and the hematopoietic cells on the lower hierarchy. The germ cell neoplasm most frequently attains the smallest evolution pseudotime, entailed by breast cancer cells and other neoplasm cells. This potentially indicates that the neoplasm cells with high frequency in rank statistics are more de-differentiated.

sample size is large. Finally, we applied our methods to datasets in several domains and showed how our Bayesian procedure leads embeddings with low distortion and allows us to quantify the uncertainty due to noise in the observed dissimilarities. In independent work issued just as we submitted this paper, [Praturu and Sharpee \(2022\)](#) also carried out a Bayesian analysis of hyperbolic MDS. The present paper builds on [Liu *et al.* \(2022\)](#). The present work differs from that of [Praturu and Sharpee \(2022\)](#) in several ways. Namely, we use priors for the latent positions in the hyperbolic space whereas [Praturu and Sharpee \(2022\)](#) assume a Gaussian noise structure on distances. Additionally, we propose using a case-control approximation to address computation whereas [Praturu and Sharpee \(2022\)](#) use an iterative approach that adds observations in blocks.

There are several avenues of interesting work. First, we have assumed in this work a low dimension for the desired embedding. While this does allow for easy visualization of the resulting embedding, imposing a low dimension on the dissimilarities is likely to lead to higher distortion than larger dimensions. One potential area of future work could derive an information criterion to estimate an optimal embedding dimension given the dissimilarities, as was done in [Oh and Raftery \(2001\)](#). Second, exploring how our proposed procedure could be adopted into the non-metric multidimensional scaling framework. Finally, while hyperbolic space has received a lot of attention in the past few years, spaces of non constant curvature, as studied in [De Sa *et al.* \(2018\)](#) and others, might lead to an embedding with lower distortions. An interesting research question here could focus on proposing Bayesian MDS methods in these spaces.

References

- I. Borg and P. Groenen. *Modern Multidimensional Scaling*. New York: Springer-Verlag, 1997.
- I. Chami, A. Wolf, D.-C. Juan, F. Sala, S. Ravi, and C. Ré. Low-dimensional hyperbolic knowledge graph embeddings. *arXiv preprint arXiv: 2005.00545*, 01 2020.
- T. F. Cox and M. A. A. Cox. *Multidimensional Scaling*. London: Chapman Hall, 2001.
- M. L. Davison. *Multidimensional Scaling*. New York: Wiley, 1983.
- C. De Sa, A. Gu, C. Ré, and F. Sala. Representation tradeoffs for hyperbolic embeddings. *Proceedings of Machine Learning Research*, 80, 04 2018.

- P. Doreian. Exploratory social network analysis with Pajek, W. de nooy, A. Mrvar, V. Batagelj. Cambridge University Press, New York (2005). *Social Networks*, 28:269–274, 07 2006.
- M. Elowitz, A. Levine, E. Siggia, and P. Swain. Stochastic gene expression in a single cell. *Science (New York, N.Y.)*, 297:1183–6, 09 2002.
- T. Fonseca, H. Migon, and M. Ferreira. Bayesian analysis based on the jeffreys prior for the hyperbolic distribution. *Brazilian Journal of Probability and Statistics*, 26, 11 2012.
- D. Friedmann-Morvinski and I. Verma. Dedifferentiation and reprogramming: Origins of cancer stem cells. *EMBO reports*, 15, 03 2014.
- T. Gneiting, F. Balabdaoui, and A. Raftery. Probabilistic forecasts, calibration and sharpness. *Journal of the Royal Statistical Society: Series B (Statistical Methodology)*, 69:243 – 268, 04 2007.
- P. J. F. Groenen. *The Majorization Approach to Multidimensional Scaling: Some Problems and Extensions*. Liden, The Netherlands: DSWO, 1993.
- W. Hofbauer, L. Forrest, P. Hollingsworth, and M. Hart. Preliminary insights from DNA barcoding into the diversity of mosses colonising modern building surfaces. *Bryophyte Diversity and Evolution*, 38:1, 04 2016.
- P. D. Hoff, A. E. Raftery, and M. S. Handcock. Latent space approaches to social network analysis. *Journal of the American Statistical Association*, 2002.
- A. J. Holbrook, P. Lemey, G. Baele, S. Dellicour, D. Brockmann, A. Rambaut, and M. A. Suchard. Massive parallelization boosts big Bayesian multidimensional scaling. *Journal of Computational and Graphical Statistics*, 30:11–24, 2021.
- M. Keller-Ressel and S. Nargang. Hydra: a method for strain-minimizing hyperbolic embedding of network- and distance-based data. *Journal of Complex Networks*, 8, 02 2020.
- A. Klimovskaia, D. Lopez-Paz, L. Bottou, and M. Nickel. Poincaré maps for analyzing complex hierarchies in single-cell data. *Nature Communications*, 11, 06 2020.

- J. B. Kruskal. Multidimensional scaling by optimizing goodness of fit to a nonmetric hypothesis. *Psychometrika*, 29(1):1–27, 1964.
- B. Liu, S. Lubold, A. Raftery, and T. McCormick. Bayesian hyperbolic multidimensional scaling. *Presentation at the Joint Statistical Meetings, Washington, D.C.*, August 2022.
- S. Lubold, A. Chandrasekhar, and T. McCormick. Identifying the latent space geometry of network models through analysis of curvature. *arXiv preprint arXiv:2012.10559*, 2020.
- M. Lukk, M. Kapushesky, J. Nikkilä, H. Parkinson, A. Goncalves, W. Huber, E. Ukkonen, and A. Brazma. A global map of human gene expression. *Nature Biotechnology*, 28:322–4, 04 2010.
- D. MacKay. Probabilistic multidimensional scaling: An anisotropic model for distance judgements. *Marketing Science*, 5:325–334, 1989.
- Y. Nagano, S. Yamaguchi, Y. Fujita, and M. Koyama. A wrapped normal distribution on hyperbolic space for gradient-based learning. *arXiv preprint arXiv: 1902.02992*, 2019.
- M. Nickel and D. Kiela. Poincaré embeddings for learning hierarchical representations. *arXiv preprint arXiv: 1705.08039*, 05 2017.
- M.-S. Oh and A. E. Raftery. Bayesian multidimensional scaling and choice of dimension. *Journal of the American Statistical Association*, 96(455):1031–1044, 2001.
- M. Oleksiak, G. Churchill, and D. Crawford. Variation in gene expression within and among natural populations. *Nature Genetics*, 32:261–6, 11 2002.
- M. Plummer, N. Best, K. Cowles, and K. Vines. CODA: Convergence diagnosis and output analysis for MCMC. *R News*, 6(1):7–11, 2006.
- A. Praturu and T. Sharpee. A Bayesian approach to hyperbolic multi-dimensional scaling. *bioRxiv*, 2022.
- A. E. Raftery and S. M. Lewis. Comment: one long run with diagnostics: implementation strategies for Markov chain Monte Carlo. *Statistical science*, 7(4):493–497, 1992.

- A. Raftery, X. Niu, P. Hoff, and K. Y. Yeung. Fast inference for the latent space network model using a case-control approximate likelihood. *Journal of Computational and Graphical Statistics*, 21, 10 2012.
- A. Raj and A. Oudenaarden. Nature, nurture, or chance: Stochastic gene expression and its consequences. *Cell*, 135:216–26, 11 2008.
- A. L. Smith, D. M. Asta, C. A. Calder, et al. The geometry of continuous latent space models for network data. *Statistical Science*, 34(3):428–453, 2019.
- Y. Takane and J. D. Carroll. Nonmetric maximum likelihood multidimensional scaling from directional rankings of similarities. *Psychometrika*, 46:389–405, 1981.
- W. Zachary. An information flow model for conflict and fission in small groups. *Journal of anthropological research*, 33, 11 1976.
- Y. Zhou and T. Sharpee. Hyperbolic geometry of gene expression. *iScience*, 24:102225, 02 2021.

Appendices

A Reasoning of the Prior Choice

Note that, since each \mathbf{x}_i is defined on $\mathbb{H}^p(\kappa)$, we cannot apply a usual multivariate normal prior on \mathbf{X} as in [Oh and Raftery \(2001\)](#), which is originally defined on the Euclidean geometry. It is tempting to consider distributions defined on the hyperbolic space as substitutes of the multivariate normal distribution, such as the distributions described in [Fonseca *et al.* \(2012\)](#) and [Nagano *et al.* \(2019\)](#), and directly specify the prior on \mathbf{X} . However, since the hyperbolic space is centered around $\boldsymbol{\mu}_0^p = (1, 0, \dots, 0) \in \mathbb{H}^p \subset \mathbb{R}^{p+1}$ instead of the Euclidean origin $(0, \dots, 0) \in \mathbb{R}^{p+1}$, directly impose a hyperbolic prior on \mathbf{X} will generally lead to an asymmetric proposal function, and restrict us from applying the random walk Metropolis-Hastings sampling algorithm described in [Oh and Raftery \(2001\)](#), which uses a symmetric proposal function, and is more tractable and computationally efficient.

B Curvature Estimation through Stress Minimization

In this section, we define an estimate of the curvature of the $\mathbb{H}^p(\kappa)$ given (potentially) noisy dissimilarities between points on $\mathbb{H}^p(\kappa)$. An advantage of the estimator we now propose is that it does not depend on knowing the dimension p of the space. For any curvature value κ , we let $\mathbf{x}_i(\kappa)$ for $i = 1, \dots, n$ denote the set of embedding coordinates obtained from hyperbolic MDS ([Keller-Ressel and Nargang \(2020\)](#)) computed using the curvature value κ , and we let $d_{ij}(\kappa)$ be the distance between $\mathbf{x}_i(\kappa)$ and $\mathbf{x}_j(\kappa)$. Our estimate $\hat{\kappa}$ is then the estimate that minimizes the stress between the observed dissimilarities $\{\hat{\delta}_{ij}\}$ and the distances $\{d_{ij}(\kappa)\}$. That is, we set

$$\hat{\kappa} = \arg \min_{\kappa} \text{stress} \left(\{d_{ij}(\kappa)\}, \{\hat{\delta}_{ij}\} \right) =: \arg \min_{\kappa} \sqrt{\frac{\sum_{i < j} \left(d_{ij}(\kappa) - \hat{\delta}_{ij} \right)^2}{\sum_{i < j} d_{ij}(\kappa)^2}}.$$

This is not the only way to estimate curvature of $\mathbb{H}^p(\kappa)$ given (potentially) noisy dissimilarity data. [Lubold *et al.* \(2020\)](#), for example, proposed a different estimate of curvature and proved it is consistent as the error in $\{\hat{\delta}_{ij}\}$ goes to zero. But we found in simulations that the above

estimator outperforms the estimate in [Lubold *et al.* \(2020\)](#) for the noise levels we consider in this work.

C MCMC Convergence

In this section, we provide typical trace plots from our simulations and data sets. We plot the MCMC proposed δ_{ij} and σ values over iterations t for the MCMC simulation in [Section 5](#). Specifically, to comprehensively investigate the convergence of δ_{ij} , we ran a BHMDS simulation for sample size $n = 200$, hyperbolic dimension $p = 2$, error size $\sigma = 1$, with 20,000 MCMC iterations and burn-in of 3,000 iterations, randomly pick ten δ_{ij} entries from the dissimilarity matrix, and record their MCMC sampled values after the MCMC burn-in. We provide the trace plots below. We also assessed convergence using the diagnostic of [Raftery and Lewis \(1992\)](#). We analyze the traces using the default `raftery.diag()` function from the `coda` R package ([Plummer *et al.*, 2006](#)), and summarize the results in [Table 4](#). Our choice of total number of MCMC iterations is close to the average of the suggested total number of MCMC iterations, $\bar{N} = 21596$ iterations $N_{min} = 3746$. This suggests that around 20,000 MCMC iterations is enough to estimate the parameters of interest in BHMDS.

Table 4: Summary of the `raftery.diag()` MCMC diagnosis for traces of the ten δ_{ij} random samples and error size σ . M is small for all traces, indicating we burn-in enough of the MCMC samples. Our choice of total number of MCMC iterations is close to the suggested total number of MCMC iterations N 's, and greatly exceeds the suggested minimal number of iterations $Nmin$, indicating the proposed MCMC sampler mixes well with ~ 20000 MCMC iterations.

	Burn-in (M)	Total (N)	Lower bound (Nmin)	Dependence factor (I)
Sample 1	21	24222	3746	6.47
Sample 2	18	19083	3746	5.09
Sample 3	18	20487	3746	5.47
Sample 4	24	24474	3746	6.53
Sample 5	20	22194	3746	5.92
Sample 6	18	20061	3746	5.36
Sample 7	18	21762	3746	5.81
Sample 8	20	22152	3746	5.91
Sample 9	20	23348	3746	6.23
Sample 10	18	21612	3746	5.77
σ	18	18158	3746	4.85

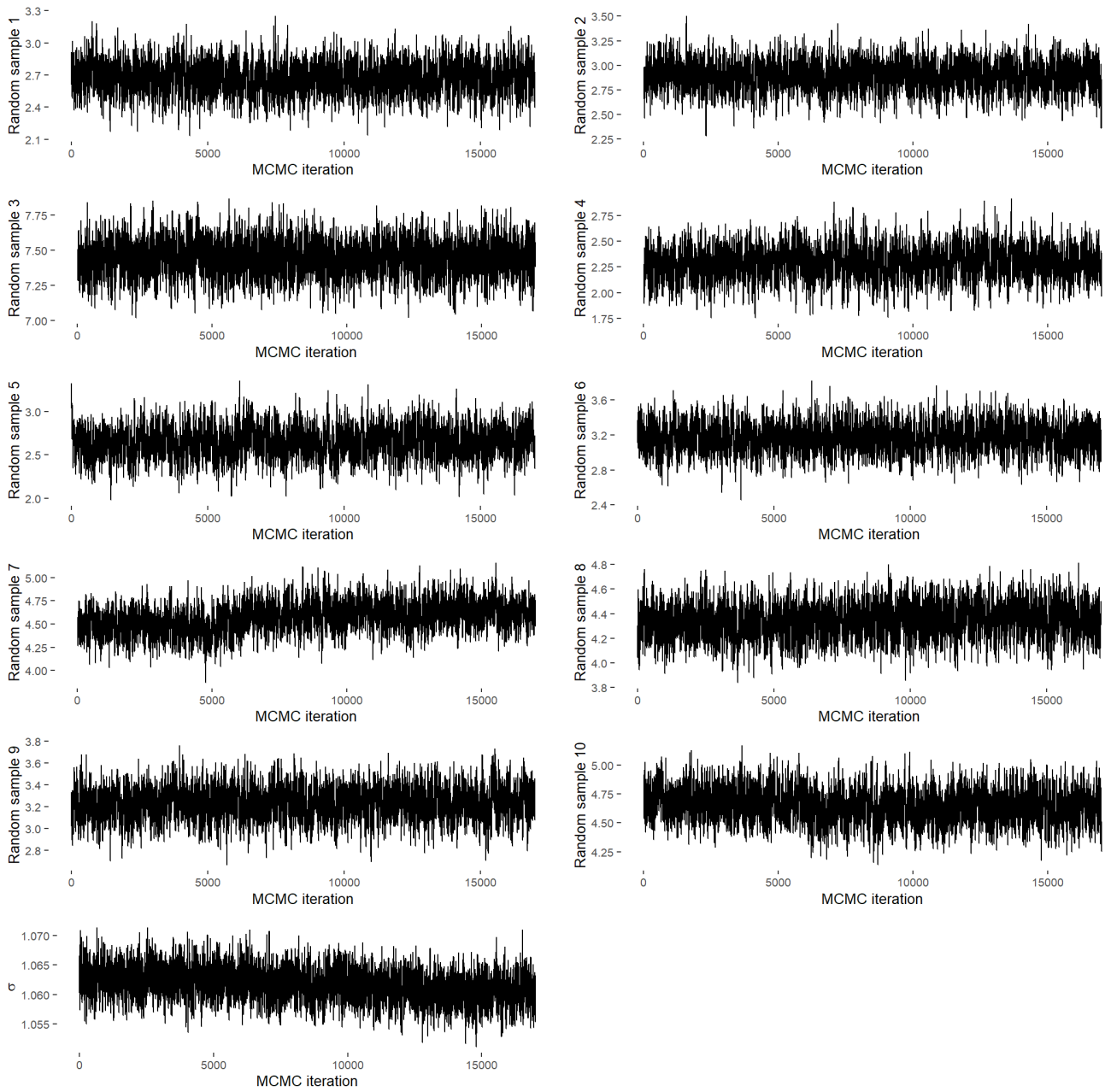


Figure C.1: Trace plots of ten randomly sampled MCMC proposed δ_{ij} and σ values over iteration t for MCMC simulation in Section 5 with $n = 200$, $p = 2$, $\sigma = 1$.